

# Fast and accurate prediction of numerical relativity waveforms from binary black hole mergers using surrogate models

Jonathan Blackman,<sup>1</sup> Scott E. Field,<sup>2</sup> Chad R. Galley,<sup>1</sup> Béla Szilágyi,<sup>1</sup> Mark A. Scheel,<sup>1</sup> Manuel Tiglio,<sup>3</sup> and Daniel A. Hemberger<sup>1</sup>

<sup>1</sup>TAPIR, Walter Burke Institute for Theoretical Physics, California Institute of Technology, Pasadena, CA 91125, USA

<sup>2</sup>Center for Radiophysics and Space Research, Cornell University, Ithaca, New York 14853, USA

<sup>3</sup>Center for Astrophysics and Space Sciences, Center for Computational Mathematics, San Diego Supercomputer Center, University of California San Diego, 9500 Gilman Drive, La Jolla, California 92093-0424, USA

(Dated: July 21, 2022)

Simulating a binary black hole coalescence by solving Einstein’s equations is computationally expensive, requiring days to months of supercomputing time. In this paper, we construct an accurate and fast-to-evaluate surrogate model for numerical relativity (NR) waveforms from non-spinning binary black hole coalescences with mass ratios from 1 to 10 and durations corresponding to about 15 orbits before merger. Our surrogate, which is built using reduced order modeling techniques, is distinct from traditional modeling efforts. We find that the full multi-mode surrogate model agrees with waveforms generated by NR to within the numerical error of the NR code. In particular, we show that our modeling strategy produces surrogates which can correctly predict NR waveforms that were *not* used for the surrogate’s training. For all practical purposes, then, the surrogate waveform model is equivalent to the high-accuracy, large-scale simulation waveform but can be evaluated in a millisecond to a second depending on the number of output modes and the sampling rate. Our model includes all spherical-harmonic  ${}_{-2}Y_{\ell m}$  waveform modes that can be resolved by the NR code up to  $\ell = 8$ , including modes that are typically difficult to model with other approaches. We assess the model’s uncertainty, which could be useful in parameter estimation studies seeking to incorporate model error. We anticipate NR surrogate models to be useful for rapid NR waveform generation in multiple-query applications like parameter estimation, template bank construction, and testing the fidelity of other waveform models.

Since the breakthroughs of 2005 [1–3], tremendous progress in numerical relativity (NR) has led to hundreds of simulations of binary black hole (BBH) coalescences [4–10]. This progress has been driven partly by data analysis needs of advanced ground-based gravitational wave detectors like LIGO [11] and Virgo [12]. Recent upgrades to these detectors are expected to yield the first direct detections of gravitational waves (GWs) from compact binary coalescences [13].

Despite the remarkable progress of the NR community, a single high-quality simulation typically requires days to months of supercomputing time. This high computational cost makes it difficult to directly use NR waveforms for data analysis, except for injection studies [4, 9], since detecting GWs and inferring their source parameters may require thousands to millions of accurate gravitational waveforms. Nevertheless, a first template bank for nonspinning binaries in Advanced LIGO has been recently constructed from NR waveforms [14]. Furthermore, NR waveforms have been used successfully in calibrating inspiral-merger-ringdown (IMR) effective-one-body (EOB) [15–21] and phenomenological [22–25] models. These models have free parameters that can be set by matching to NR waveforms and are suitable for certain GW data analysis studies [26]. However, these models can have systematic errors since they assume *a priori* physical waveform structure and are calibrated and tested against a small set of NR simulations.

In this Letter, we present an *ab initio* methodology

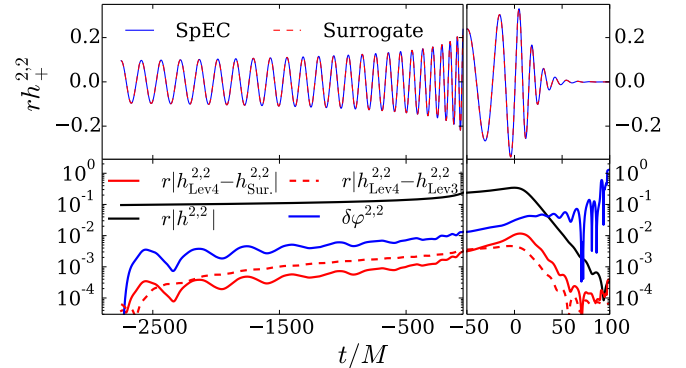


FIG. 1. **Top:** The + polarization (2,2) mode prediction for  $q = 2$ , the surrogate model’s worst prediction over  $q$  from a “leave-one-out” surrogate that was *not* trained with this waveform (see below). Our full surrogate, trained on the entire data set, is more accurate. **Bottom:** Phase  $\delta\varphi^{2,2}$  and waveform differences between the surrogate and highest resolution (Lev4) SpEC waveforms. Also shown is the SpEC numerical truncation error found by comparing the two highest resolution (Lev4 and Lev3) waveforms.

based on surrogate [27, 28] and reduced order modeling techniques [29–33] that is capable of accurately predicting the gravitational waveform outputs from NR *without* any phenomenological assumptions or approximations to general relativity. From a small set of specially selected non-spinning BBH simulations performed with the Spec-

tral Einstein Code (SpEC) [34–36], we build a surrogate model for SpEC waveforms that can be used in place of performing SpEC simulations. The techniques are general, however, and directly apply to other NR codes or even analytical waveform models. The surrogate model constructed here generates non-spinning BBH waveforms with mass ratios  $q$  in  $[1, 10]$ , contains 25–31 gravitational wave cycles before peak amplitude, and includes many spherical-harmonic modes (see Table I and its caption). These choices are made based on available NR waveforms and are not limitations of the method. Our surrogate model has errors close to the estimated numerical error of the input waveforms. An example comparison of the surrogate output to an NR waveform can be seen in Fig. 1. This simulation took 9.3 days using 48 cores but only  $\sim 0.01$  sec for the surrogate evaluation of the  $(2, 2)$  mode.

Previous work [27, 37] built surrogates for EOB waveforms; building and assessing surrogate models of NR waveforms have unique challenges associated with input waveforms that are expensive to compute. We summarize next the construction of our model, focusing on steps that were not addressed in [27] but are required for NR surrogates.

*Parametric sampling*– Typically, a surrogate model is trained on a dense set of waveforms known as the *training set*. In the case of NR, however, we cannot afford to generate a large number of waveforms. Instead, we generate a dense set of non-spinning waveforms using an EOB model [18], as implemented in [38], which contains the  $(\ell, m) = \{(2, 2), (2, 1), (3, 3), (4, 4), (5, 5)\}$  spin-weight  $-2$  spherical-harmonic modes and captures the robust features of NR waveforms. The EOB training set waveforms are computed for times in  $[-2750, 100]M$ , which is the interval over which we build our surrogates and where  $M$  is the total mass.

Next, on this training set we apply a greedy algorithm to expose the most relevant mass ratio values [39, 40]. SpEC simulations of non-spinning BBH mergers are then performed for these mass ratios. The resulting NR waveforms are used to build our surrogates without any further input from the EOB model.

We seeded the greedy algorithm with 5 publicly available SpEC simulations of non-spinning BBH mergers [10, 19] (see Table I), and the next 17 (ordered) mass ratio values are the algorithm’s output based on the EOB model. The final  $\approx 10$  mass ratios are included to improve the surrogate if necessary, since we can assess the surrogate model’s accuracy only after it is built (cf. Fig. 6). Our method for building surrogates is hierarchical [27, 40]; additional NR waveforms can be included to improve the model’s accuracy.

*Generating the NR waveforms*– Table I summarizes the 22 SpEC simulations used in this paper. See, e.g., Ref. [35] for the numerical techniques used in SpEC. The numerical resolution is denoted by “Levi”, where

| #  | ID  | $q$  | $e_{-5}$ | $T/M$ | Orbs | #  | ID  | $q$  | $e_{-5}$ | $T/M$ | Orbs |
|----|-----|------|----------|-------|------|----|-----|------|----------|-------|------|
| 1  | 180 | 1.00 | 5.1      | 9867  | 28.2 | 12 | 191 | 2.51 | 65       | 6645  | 22.5 |
| 2  | 181 | 6.00 | 5.8      | 7056  | 26.5 | 13 | 192 | 6.58 | 4.0      | 5149  | 21.1 |
| 3  | 182 | 4.00 | 12       | 3840  | 15.6 | 14 | 193 | 3.50 | 3.0      | 5242  | 19.6 |
| 4  | 183 | 3.00 | 4.8      | 4008  | 15.6 | 15 | 194 | 1.52 | 74       | 5774  | 19.6 |
| 5  | 184 | 2.00 | 15       | 4201  | 15.6 | 16 | 195 | 7.76 | 22       | 5226  | 21.9 |
| 6  | 185 | 9.99 | 31       | 5817  | 24.9 | 17 | 196 | 9.66 | 23       | 5330  | 23.1 |
| 7  | 186 | 8.27 | 16       | 5687  | 23.7 | 18 | 197 | 5.52 | 25       | 5061  | 20.3 |
| 8  | 187 | 5.04 | 3.0      | 4807  | 19.2 | 19 | 198 | 1.20 | 17       | 6315  | 20.7 |
| 9  | 188 | 7.19 | 15       | 5439  | 22.3 | 20 | 199 | 8.73 | 8.5      | 5302  | 22.6 |
| 10 | 189 | 9.17 | 13       | 6019  | 25.2 | 21 | 200 | 3.27 | 36       | 5507  | 20.2 |
| 11 | 190 | 4.50 | 2.5      | 5199  | 20.1 | 22 | 201 | 2.32 | 15       | 5719  | 20.0 |

TABLE I. Properties of the highest resolution SpEC simulations used for building binary black hole waveform surrogates. The orbital eccentricity  $e_{-5}/10^5$  is measured after initial transients have left the computational grid. The duration  $T/M$  and number of orbits (Orbs) are also given. The SpEC simulations are available in the public waveform catalog [10] under the name “SXS:BBH:ID.”

$i$  is an integer that controls the truncation error allowed by adaptive mesh refinement in SpEC; larger numbers correspond to smaller errors and more computationally-expensive simulations. Two to five levels of resolution are simulated for each mass ratio. To achieve quasi-circular orbits, initial data is subject to an iterative eccentricity reduction procedure resulting in eccentricities  $\lesssim 7 \times 10^{-4}$  [41–43].

SpEC numerically solves an initial boundary value problem defined on a finite computational domain. An observation in the radiation zone, however, is well approximated as taking place at future null infinity  $\mathcal{I}^+$ . To obtain waveforms at  $\mathcal{I}^+$ , we use the Cauchy characteristic extraction (CCE) method [44–48]. Using the PittNull code [44–46], we compute the Newman-Penrose scalar  $\Psi_4$  at  $\mathcal{I}^+$  and finally obtain the gravitational wave strain  $h$  through two temporal integrations. We minimize the low-frequency, noise-induced “drifts” [47] by using frequency cut-offs<sup>1</sup>

Figure 2 shows the convergence typically observed in our simulations. Although textbook convergence is difficult to achieve in production SpEC simulations (see the discussion in Sec. IIIB of [35]), waveform differences typ-

<sup>1</sup> We integrate  $\Psi_4$  twice in the (dimensionless) frequency domain by dividing  $-\Psi_4^{\ell,m}(f)$  by  $[2\pi \max(f, 2f_0/3)]^2$ , where  $f_0$  is the initial GW mode frequency. For the  $(2, 0)$  mode, which has high power from low frequencies, we hybridize  $\Psi_4^{2,0}$  with a corresponding Taylor T4 post-Newtonian inspiral waveform mode from  $600M$  to  $100M$  before merger where  $\Psi_4^{2,0}$  begins to rise above the SpEC truncation error. Our surrogate is built from and compared to  $h^{2,0}$  stemming from hybridized data  $\Psi_4^{2,0}$ .

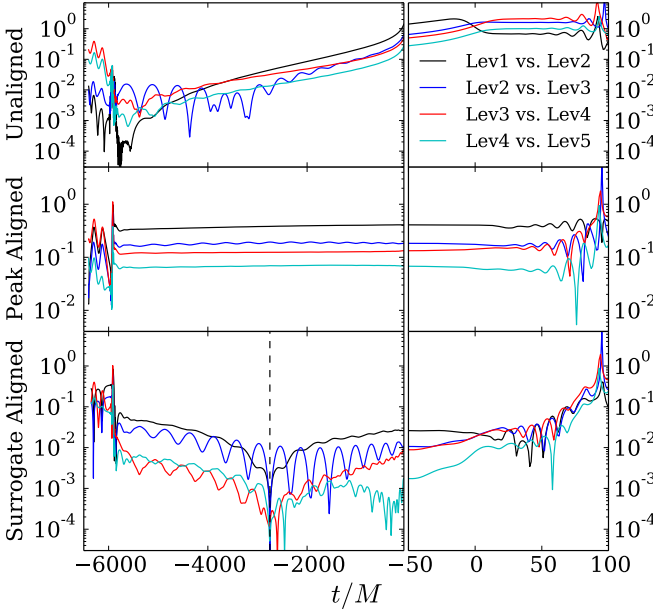


FIG. 2. The relative error,  $|h_i^{22} - h_{i+1}^{22}|/|h_{i+1}^{22}|$ , of successive resolutions SpEC Levi for the (2,2) mode of simulation 19 in Table I. **Top:** Waveform output as directly given by SpEC (“Unaligned”). **Middle:** Peak-aligned waveforms where a Lev-dependent time shift is applied to set all peaks to  $t = 0$ . **Bottom:** “Surrogate aligned,” which involves a rotation of the binary around the  $z$ -axis to align the waveform phases at the surrogate’s initial time  $t_i = -2750M$  together with the peak alignment scheme.

ically decrease quickly with increasing resolution. Let

$$\delta h^{\ell,m}(q) \equiv \frac{\|h_1^{\ell,m}(\cdot; q) - h_2^{\ell,m}(\cdot; q)\|^2}{\sum_{\ell,m} \|h_2^{\ell,m}(\cdot; q)\|^2} \quad (1)$$

be the disagreement between two waveform modes  $h_1^{\ell,m}$  and  $h_2^{\ell,m}$  where  $\|h^{\ell,m}(\cdot; q)\|^2 = \int dt |h^{\ell,m}(t; q)|^2$ . We estimate the numerical truncation error of each mode when  $h_1$  and  $h_2$  are waveforms computed at the two highest resolutions. The full waveform error for a given mass ratio is  $\delta h(q) = \sum_{\ell,m} \delta h^{\ell,m}(q)$ . We also report errors after an overall simulation-dependent time shift and rotation (called “surrogate aligned”, described in the next section), which are physically unimportant coordinate changes. The resulting estimated numerical truncation errors of the dominant (2,2) modes, using our surrogate alignment scheme, are shown in Fig. 3 (black circles).

Additional error sources are non-zero eccentricity in the (intended to be circular) NR initial data, and an imperfect procedure for integrating  $\Psi_4^{\ell,m}$  to obtain  $h^{\ell,m} \equiv A^{\ell,m} \exp(-i\varphi^{\ell,m})$ . These both cause small oscillations in the waveform amplitudes  $A^{\ell,m}(t)$  and phases  $\varphi^{\ell,m}(t)$  [47, 49] that we model following [49]. We also compute the error in the strain integration scheme by comparing  $\Psi_4^{\ell,m}$  to two time derivatives of  $h^{\ell,m}$ , as well as estimates for numerical errors in the CCE method [48].

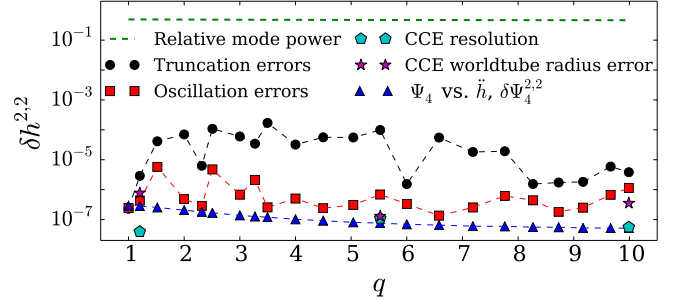


FIG. 3. Numerical truncation errors (black) dominate all other sources of error for the (2,2) mode, except for simulation 1 ( $q \approx 1$ ), where the truncation errors are already very small. For some weaker modes, systematic amplitude oscillations primarily due to eccentricity may become more relevant.

For the (2,2) mode, these additional errors are negligibly small compared to SpEC truncation errors (cf. Fig. 3).

*Preparing NR waveforms for surrogate modeling*– We apply a simulation-dependent time shift and physical rotation about the  $z$ -axis so that all the modes’ phases are aligned. This reveals the underlying parametric smoothness in  $q$  that will be useful for building a surrogate. Our time shifts set each waveform’s *total* amplitude

$$A(t; q)^2 \equiv \int_{S^2} d\Omega |h(t, \theta, \phi; q)|^2 = \sum_{\ell,m} |h^{\ell,m}(t; q)|^2, \quad (2)$$

to be maximum at  $t = 0$ . After enforcing this alignment scheme we interpolate the waveform mode amplitudes and phases onto an array of uniformly spaced times in  $[-2750, 100]M$ , with  $\Delta t = 0.1M$ . Finally, we align the initial gravitational wave mode phases by performing a simulation-dependent, constant (in time) physical rotation about the  $z$ -axis so that  $\varphi^{2,2}(t_i) = \varphi^{2,-2}(t_i)$ , which fixes a physical rotation up to multiples of  $\pi$ . We resolve the ambiguity by requiring  $\varphi^{2,1}(t_i) \in (-\pi, 0]$ . Waveform truncation errors, after performing this *surrogate alignment* scheme, are shown in Fig. 2. In what follows, we call “truncation error after surrogate alignment” simply “truncation error.”

*Building the surrogate*– Each  $m \geq 0$  mode,  $h^{\ell,m}(t; q)$ , is modeled separately while (due to reflection symmetry about the orbital plane)  $m < 0$  modes are evaluated using  $h^{\ell,-m}(t; q) = (-1)^\ell h^{\ell,m}(t; q)^*$ . We do not model modes which do not improve the predictive power of the surrogate. Table II lists our modeled modes and their errors.

Our complete surrogate waveform model is defined by  $h_S(t, \theta, \phi; q) = \sum_{\ell,m} h_S^{\ell,m}(t; q) {}_{-2}Y_{\ell m}(\theta, \phi)$  where

$$h_S^{\ell,m}(t; q) = A_S^{\ell,m}(t; q) e^{-i\varphi_S^{\ell,m}(t; q)}, \quad (3)$$

$$X_S^{\ell,m}(t; q) = \sum_{i=1}^{N_X} B_{X,i}^{\ell,m}(t) X_i^{\ell,m}(q), \quad X = \{A, \varphi\}.$$

Unlike Ref. [27], we construct a reduced basis representation for the waveform amplitudes and phases separately, instead of the waveforms themselves [37]. Here, the  $\{B_{X,i}^{\ell m}\}_{i=1}^{N_X}$  are computed off-line from the SpEC waveforms [27]. At a set of  $N_X$  specially selected times  $\{T_{X,i}^{\ell m}\}_{i=1}^{N_X}$ , which are the empirical interpolant nodes [27, 50], the functions  $X_i^{\ell m}(q) \approx X^{\ell m}(T_{X,i}^{\ell m}; q)$  approximate the parametric variation of the amplitudes and phases (via fitting, see below). A thorough discussion of surrogate model building steps is presented in [27]. When evaluating the surrogate at a particular mass ratio, the fits are evaluated first to determine the amplitudes and phases at their respective interpolating times  $\{T_{X,i}^{\ell m}\}_{i=1}^{N_X}$ . The remaining operations yield the surrogate model prediction,  $h_S(t, \theta, \phi; q)$ .

To find each  $X_i^{\ell m}(q)$  we perform least-squares fits to the 22 data points,  $\{X^{\ell m}(T_{X,i}^{\ell m}; q_j)\}_{j=1}^{22}$ . All fits except odd  $m$  mode amplitudes use 5th degree polynomials in the symmetric mass ratio,  $\nu = q/(1+q)^2$ . For odd  $m$  modes, the amplitude approaches 0 and its derivative with respect to  $\nu$  diverges as  $q \rightarrow 1$  (or  $\nu \rightarrow 1/4$ ). Consequently, we use  $A_i^{\ell m}(\nu) = \sum_{n=1/2,1}^5 a_n^{\ell m} (1-4\nu)^n$  to account for this behavior. The waveform phases of odd  $m$  modes at  $q = 1$ , which are undefined, are excluded when fitting for each  $\varphi_i^{\ell m}(q)$ .

*Assessing surrogate errors*— We next assess the surrogate’s predictive quality. To quantify the error in the surrogate model itself, as opposed to its usage in a data analysis study, we do *not* minimize the errors over relative time and phase shifts for any of these studies.

A first test is a consistency check to reproduce the 22 input SpEC waveforms used to build the surrogate. These errors are shown in Fig. 4 (red squares) and are comparable to SpEC truncation errors (black circles).

A more stringent test is the leave-one-out cross-validation (LOOCV) study [51]. For each simulated mass ratio  $q_i$ , we build a temporary *trial surrogate* using the other 21 waveforms, evaluate the trial surrogate at  $q_i$ , and compare the prediction with the SpEC waveform for  $q_i$ . Hence, the trial surrogate’s error at  $q_i$  should serve as an upper bound for the full surrogate trained on all 22 waveforms. Repeating this process for all possible 20 LOOCV tests<sup>2</sup> results in Fig. 4 (blue triangles). Despite the  $i$ th trial surrogate having no information about the waveform at  $q_i$ , the errors remain comparable to the SpEC truncation errors. The LOOCV errors are typically twice as large as the full surrogate ones confirming the former as bounds for the latter. Relative errors for selected modes are shown in Table II. While weaker modes have larger relative errors, their power contribution is small enough that the error in the full surrogate waveform,  $\delta h$ , is nearly

| $(\ell, m)$ | Surrogate |      | NR   |      | $(\ell, m)$ | Surrogate |      | NR   |      |
|-------------|-----------|------|------|------|-------------|-----------|------|------|------|
|             | Max       | Mean | Max  | Mean |             | Max       | Mean | Max  | Mean |
| (2, 2)      | 0.36      | 0.07 | 0.36 | 0.08 | (3, 2)      | 100       | 17   | 1.7  | 0.43 |
| (2, 1)      | 29        | 3.4  | 4.1  | 0.54 | (4, 4)      | 7.4       | 2.2  | 20   | 2.1  |
| (2, 0)      | 2.1       | 0.27 | 0.04 | 0.01 | (5, 5)      | 5.4       | 3.1  | 1.0  | 0.33 |
| (3, 3)      | 53        | 4.1  | 11   | 0.94 | All         | 0.41      | 0.12 | 0.40 | 0.10 |

TABLE II. Relative mode errors, reported as  $10^3 \times \|h_S^{\ell, m}(q) - h^{\ell, m}(q)\|^2 / \|h^{\ell, m}(q)\|^2$ , from the leave-one-out surrogates. Only those modes which contribute greater than 0.02% to the full waveform’s time-domain power are used in the computation of the max and mean, except for ‘All’ which is just  $\delta h$ . Our surrogate also includes the (3, 1), (4, [2, 3]), (5, [3, 4]), (6, [4, 5, 6]), (7, [5, 6, 7]), and (8, [7, 8]) modes. Weaker modes typically have relative errors between 1% and 35%.

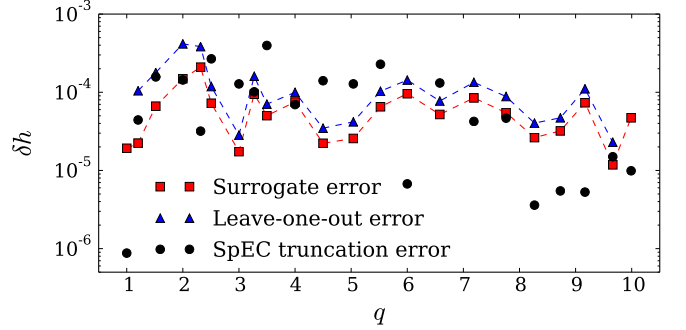


FIG. 4. Waveform differences between the two highest SpEC resolutions (black circles), the full surrogate and SpEC (red squares), and leave-one-out trial surrogates and SpEC (blue triangles). The largest surrogate error is for  $q = 2$ , for which the (2, 2) mode is shown in Fig. 1.

identical to the SpEC resolution error.

A third test is to compare the surrogate waveforms to those of a second surrogate, built from the second highest resolution SpEC waveforms. The resulting comparison (solid lines) is shown for the full waveform and several of its modes in Fig. 5. These errors are comparable to SpEC waveform truncation errors (circles). We find that the surrogate building process is robust to resolution differences. Furthermore, the surrogate can be improved using NR waveforms of higher accuracy.

We perform a final test by constructing surrogates using the first  $N$  selected mass ratios (from Table I) as input waveforms. This leaves  $22 - N$  mass ratios with which to test. For these smaller surrogates, we use fits with  $\min(N - 1, 6)$  coefficients where  $N$  is the number of input waveforms. The resulting errors are shown in Fig. 6. We see that the total waveform error becomes comparable to the SpEC truncation error for surrogates using at least 7 waveforms. However, some modes (e.g., (3, 3)) require more waveforms to be fully resolved.

*Discussion*— We have built a surrogate model for NR non-spinning BBH merger waveforms generated by

<sup>2</sup> We omit the smallest and largest mass ratios here as the corresponding trial surrogates would extrapolate to their values.



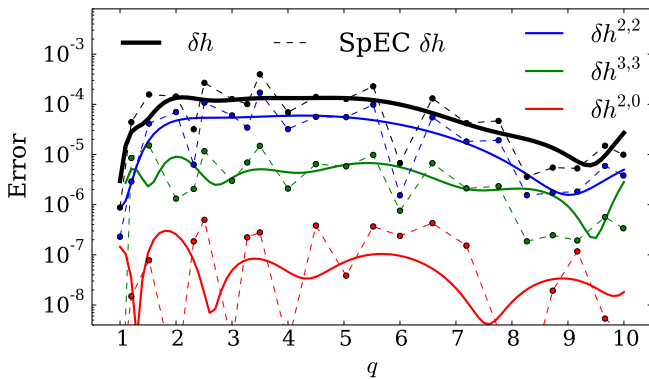


FIG. 5. Difference between the full, high-resolution surrogate and a surrogate built using the *second* highest resolution SpEC waveforms (solid curves), each evaluated at 91 mass ratios. Differences between the two highest-resolution SpEC waveforms are shown as circles and connected by a dashed line for visual assistance.

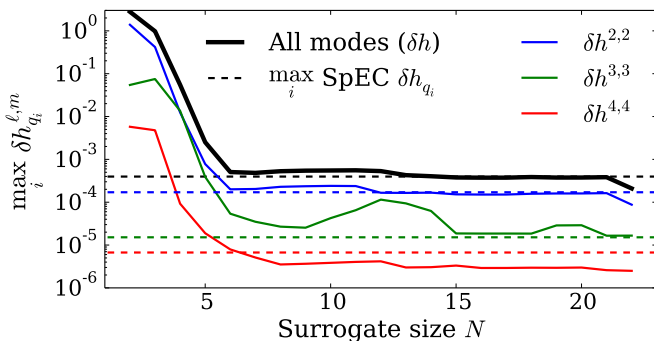


FIG. 6. Maximum errors over all 22 mass ratios for surrogates built from  $N$  SpEC waveforms. Convergence is achieved after  $\approx 7$  waveforms. The observed exponential error decay is expected for any parametrically smooth waveform family [39].

SpEC. On a standard 2015 single core computer, all 77 modes with  $2 \leq \ell \leq 8$  are evaluated in  $\approx 0.5$  sec ( $\approx 0.01$  sec for a single mode) providing a factor of  $\sim 10^6$ – $10^8$  speedup compared to SpEC. Importantly, this is achieved *without sacrificing accuracy*. Like other data-driven modeling strategies, our surrogate is valid only within the training intervals, namely,  $q \in [1, 10]$  and  $t/M \in [-2570, 100]$ . Therefore, within the training intervals, our surrogate model generates BBH merger waveforms that are equivalent to SpEC outputs *within numerical error*.

NR surrogates can be used for multiple-query applications in gravitational wave data analysis such as detector-specific template-bank (re-)generation and parameter estimation. Our surrogate, and more generally the results of this paper, open up the exciting possibility of performing, for example, parameter estimation with multi-modal NR waveforms (with hybridization, if needed). Parameter estimation studies seeking to incorporate model error may benefit from the surrogate’s relatively straight-

forward characterization and assessment of uncertainty from a combination of the surrogate’s and SpEC’s systematic and numerical errors. We anticipate NR surrogate modeling to complement traditional strategies [15–24, 26] by providing unlimited high-fidelity approximations of NR waveforms with which to calibrate, refine and make comparisons. Building NR surrogates of precessing BBH merger waveforms, which may be modeled from the parameters specially selected in [52], offer a promising avenue for modeling the full 7 dimensional BBH parameter space. The surrogate model described in this paper will be available for download after peer review at [53].

We thank Mike Boyle, Alessandra Buonanno, Jan Hesthaven, Jason Kaye, Geoffrey Lovelace, Lee Lindblom, Tom Lored, Christian Ott, Yi Pan, Harald Pfeiffer, Rory Smith, and Nicholas Taylor for many useful discussions throughout this project. This work was supported in part by NSF grants CAREER PHY-0956189, PHY-1068881, PHY-1005655, PHY-1440083, PHY-1404569, and AST-1333520 to Caltech, NSF grants PHY-1306125 and AST-1333129 to Cornell University, NSF grant PHY-1500818 to the University of California at San Diego, NSF grants PHY-1208861 and PHY-1316424 to the University of Maryland (UMD), NSERC of Canada, and the Sherman Fairchild Foundation. Computations were performed on the Zwicky cluster at Caltech, which is supported by the Sherman Fairchild Foundation and by NSF award PHY-0960291. Portions of this research were carried out at the Center for Scientific Computation and Mathematical Modeling cluster at UMD.

- 
- [1] F. Pretorius, *Phys. Rev. Lett.* **95**, 121101 (2005), [arXiv:gr-qc/0507014 \[gr-qc\]](#).
  - [2] M. Campanelli, C. Lousto, P. Marronetti, and Y. Zlochower, *Phys. Rev. Lett.* **96**, 111101 (2006), [arXiv:gr-qc/0511048 \[gr-qc\]](#).
  - [3] J. G. Baker, J. Centrella, D.-I. Choi, M. Koppitz, and J. van Meter, *Phys. Rev. Lett.* **96**, 111102 (2006), [arXiv:gr-qc/0511103 \[gr-qc\]](#).
  - [4] B. Aylott, J. G. Baker, W. D. Boggs, M. Boyle, P. R. Brady, *et al.*, *Class. Quant. Grav.* **26**, 165008 (2009), [arXiv:0901.4399 \[gr-qc\]](#).
  - [5] P. Ajith, M. Boyle, D. A. Brown, B. Bruggmann, L. T. Buchman, *et al.*, *Class. Quantum Grav.* **29**, 124001 (2012).
  - [6] A. H. Mroue, M. A. Scheel, B. Szilagyi, H. P. Pfeiffer, M. Boyle, D. A. Hemberger, L. E. Kidder, G. Lovelace, S. Ossokine, N. W. Taylor, A. Zenginoglu, L. T. Buchman, T. Chu, E. Foley, M. Giesler, R. Owen, and S. A. Teukolsky, *Phys. Rev. Lett.* **111**, 241104 (2013), [arXiv:1304.6077 \[gr-qc\]](#).
  - [7] I. Hinder *et al.* (The NRAR Collaboration), *Classical and Quantum Gravity* **31**, 025012 (2014), [arXiv:1307.5307 \[gr-qc\]](#).
  - [8] L. Pekowsky, R. O’Shaughnessy, J. Healy, and D. Shoemaker, *Phys. Rev. D* **88**, 024040 (2013), [arXiv:1304.3176](#)

- [gr-qc].
- [9] J. Aasi *et al.* (The LIGO Scientific Collaboration, the Virgo Collaboration, the NINJA-2 Collaboration), *Class. Quantum Grav.* **31**, 115004 (2014), [arXiv:1401.0939 \[gr-qc\]](#).
- [10] <http://www.black-holes.org/waveforms> ().
- [11] G. M. Harry (for the LIGO Scientific Collaboration), *Class. Quantum Grav.* **27**, 084006 (2010).
- [12] The Virgo Collaboration, “Advanced Virgo Baseline Design,” (2009), [VIR-0027A-09].
- [13] J. Abadie, B. P. Abbott, R. Abbott, M. Abernathy, T. Accadia, F. Acernese, C. Adams, R. Adhikari, P. Ajith, B. Allen, and *et al.*, *Classical and Quantum Gravity* **27**, 173001 (2010), [arXiv:1003.2480 \[astro-ph.HE\]](#).
- [14] P. Kumar, I. MacDonald, D. Brown, H. Pfeiffer, K. Cannon, M. Boyle, L. Kidder, A. Mroue, M. Scheel, B. Szilágyi, and A. Zenginoglu, *Phys. Rev. D* **89**, 042002 (2014), [1310.7949](#).
- [15] A. Buonanno and T. Damour, *Phys. Rev. D* **59**, 084006 (1999), [arXiv:gr-qc/9811091 \[gr-qc\]](#).
- [16] T. Damour and A. Nagar, *Phys. Rev. D* **79**, 081503 (2009), [arXiv:0902.0136 \[gr-qc\]](#).
- [17] A. Buonanno, Y. Pan, H. P. Pfeiffer, M. A. Scheel, L. T. Buchman, and L. E. Kidder, *Phys. Rev. D* **79**, 124028 (2009), [arXiv:0902.0790 \[gr-qc\]](#).
- [18] Y. Pan, A. Buonanno, L. T. Buchman, T. Chu, L. E. Kidder, H. P. Pfeiffer, and M. A. Scheel, *Phys. Rev. D* **81**, 084041 (2010), [arXiv:0912.3466 \[gr-qc\]](#).
- [19] Y. Pan, A. Buonanno, M. Boyle, L. T. Buchman, L. E. Kidder, *et al.*, *Phys. Rev. D* **84**, 124052 (2011), [arXiv:1106.1021 \[gr-qc\]](#).
- [20] T. Damour, A. Nagar, and S. Bernuzzi, *Phys. Rev. D* **87**, 084035 (2013), [arXiv:1212.4357 \[gr-qc\]](#).
- [21] A. Taracchini, Y. Pan, A. Buonanno, E. Barausse, M. Boyle, T. Chu, G. Lovelace, H. P. Pfeiffer, and M. A. Scheel, *Phys. Rev. D* **86**, 024011 (2012), [arXiv:1202.0790 \[gr-qc\]](#).
- [22] P. Ajith, S. Babak, Y. Chen, M. Hewitson, B. Krishnan, J. T. Whelan, B. Brügmann, P. Diener, J. Gonzalez, M. H. S. Husa, M. Koppitz, D. Pollney, L. Rezzolla, L. Santamaría, A. M. Sintes, U. Sperhake, and J. Thornburg, *Class. Quantum Grav.* **24**, S689 (2007), [arXiv:0704.3764 \[gr-qc\]](#).
- [23] L. Santamaría, F. Ohme, P. Ajith, B. Brügmann, N. Domband, M. Hannam, S. Husa, P. Mösta, D. Pollney, C. Reisswig, E. L. Robinson, J. Seiler, and B. Krishnan, *Phys. Rev. D* **82**, 064016 (2010), [arXiv:1005.3306 \[gr-qc\]](#).
- [24] R. Sturani, S. Fischetti, L. Cadonati, G. Guidi, J. Healy, *et al.*, *J. Phys. Conf. Ser.* **243**, 012007 (2010), [arXiv:1005.0551 \[gr-qc\]](#).
- [25] M. Hannam, P. Schmidt, A. Boh, L. Haegel, S. Husa, *et al.*, *Phys. Rev. Lett.* **113**, 151101 (2014), [arXiv:1308.3271 \[gr-qc\]](#).
- [26] J. Abadie *et al.* (The LIGO Scientific Collaboration and the Virgo Collaboration), *Phys. Rev. D* **83**, 122005 (2011), [arXiv:1102.3781 \[gr-qc\]](#).
- [27] S. E. Field, C. R. Galley, J. S. Hesthaven, J. Kaye, and M. Tiglio, *Phys. Rev. X* **4**, 031006 (2014), [arXiv:1308.3565 \[gr-qc\]](#).
- [28] J. Kaye, *The interpolation of gravitational waveforms*, Ph.D. thesis, Brown University (2012).
- [29] Y. Maday, A. T. Patera, and G. Turinici, *J. Sci. Comput.* **17**, 437 (2002).
- [30] K. Veroy, C. Prud’homme, and A. T. Patera, *Comptes Rendus Mathématique* **337**, 619 (2003).
- [31] C. Prud’homme, D. V. Rovas, K. Veroy, L. Machiels, Y. Maday, A. T. Patera, and G. Turinici, *Journal of Fluids Engineering* **124**, 70 (2002).
- [32] Y. Chen, J. S. Hesthaven, Y. Maday, and J. Rodríguez, *SIAM J. Sci. Comput.* **32**, 970 (2010).
- [33] A. Quarteroni, G. Rozza, and A. Manzoni, *Journal of Mathematics in Industry* **1**, 1 (2011).
- [34] <http://www.black-holes.org/SpEC.html>.
- [35] M. A. Scheel, M. Giesler, D. A. Hemberger, G. Lovelace, K. Kuper, M. Boyle, and B. Szilágyi, (2014), submitted to *Class. Quantum Grav.*, [arXiv:1412.1803 \[gr-qc\]](#).
- [36] B. Szilágyi, *Int. J. Mod. Phys. D* **23**, 1430014 (2014), [arXiv:1405.3693 \[gr-qc\]](#).
- [37] M. Pürrer, *Class. Quantum Grav.* **31**, 195010 (2014), [arXiv:1402.4146 \[gr-qc\]](#).
- [38] L. S. Collaboration, “LSC Algorithm Library software packages LAL, LALWRAPPER, and LALAPPS,” .
- [39] P. Binev, A. Cohen, W. Dahmen, R. A. DeVore, G. Petrova, and P. Wojtaszczyk, *SIAM J. Math. Analysis* **43**, 1457 (2011).
- [40] S. E. Field, C. R. Galley, F. Herrmann, J. S. Hesthaven, E. Ochsner, *et al.*, *Phys. Rev. Lett.* **106**, 221102 (2011), [arXiv:1101.3765 \[gr-qc\]](#).
- [41] H. P. Pfeiffer, D. A. Brown, L. E. Kidder, L. Lindblom, G. Lovelace, and M. A. Scheel, *Class. Quantum Grav.* **24**, S59 (2007), [gr-qc/0702106](#).
- [42] A. Buonanno, L. E. Kidder, A. H. Mroué, H. P. Pfeiffer, and A. Taracchini, *Phys. Rev. D* **83**, 104034 (2011), [arXiv:1012.1549 \[gr-qc\]](#).
- [43] A. H. Mroué and H. P. Pfeiffer, (2012), [arXiv:1210.2958 \[gr-qc\]](#).
- [44] N. T. Bishop, R. Gomez, L. Lehner, M. Maharaj, and J. Winicour, *Phys. Rev. D* **56**, 6298 (1997), [arXiv:gr-qc/9708065](#).
- [45] M. C. Babiuc, B. Szilágyi, J. Winicour, and Y. Zlochower, *Phys. Rev. D* **84**, 044057 (2011), [arXiv:1011.4223 \[gr-qc\]](#).
- [46] J. Winicour, *Living Rev. Rel.* **12** (2009).
- [47] C. Reisswig and D. Pollney, *Class. Quant. Grav.* **28**, 195015 (2011), [arXiv:1006.1632 \[gr-qc\]](#).
- [48] N. W. Taylor, M. Boyle, C. Reisswig, M. A. Scheel, T. Chu, L. E. Kidder, and B. Szilágyi, *Phys. Rev. D* **88**, 124010 (2013), [arXiv:1309.3605 \[gr-qc\]](#).
- [49] A. H. Mroué, H. P. Pfeiffer, L. E. Kidder, and S. A. Teukolsky, *Phys. Rev. D* **82**, 124016 (2010), [arXiv:1004.4697 \[gr-qc\]](#).
- [50] Y. Maday, N. C. Nguyen, A. T. Patera, and S. H. Pau, *Communications on Pure and Applied Analysis* **8**, 383 (2009).
- [51] T. Hastie, R. Tibshirani, and J. Friedman, *The Elements of Statistical Learning*, Springer Series in Statistics (Springer New York Inc., New York, NY, USA, 2001).
- [52] J. Blackman, B. Szilágyi, C. R. Galley, and M. Tiglio, *Phys. Rev. Lett.* **113**, 021101 (2014), [arXiv:1401.7038 \[gr-qc\]](#).
- [53] “Simulating eXtreme Spacetimes,” (), <http://www.black-holes.org/>.